Flat metasurfaces to focus electromagnetic waves in reflection geometry

Xin Li,[1] Shiyi Xiao,[1] Bengeng Cai,[2] Qiong He,[1] Tie Jun Cui,[2] and Lei Zhou[1,*]

[1]*State Key Laboratory of Surface Physics and Key Laboratory of Micro and Nano Photonic Structures (Ministry of Education), Fudan University, Shanghai 200433, China*

[2]*State Key Laboratory of Millimeter Waves and Institute of Target Characteristics and Identification, Southeast University, Nanjing 210096, China*

**Corresponding author: phzhou@fudan.edu.cn*

Received August 30, 2012; revised October 29, 2012; accepted November 5, 2012; posted November 6, 2012 (Doc. ID 175140); published November 28, 2012

We show that a *flat* metasurface with a *parabolic* reflection-phase distribution can focus an impinging *plane* wave to a point image in reflection geometry. Our system is much thinner than conventional geometric-optics devices and does not suffer the energy-loss issues encountered by many metamaterial devices working in transmission geometry. We designed realistic microwave samples and performed near-field scanning experiments to verify the focusing effect. Experimental results are in good agreement with full wave simulations, model calculations, and theoretical analyses. © 2012 Optical Society of America

OCIS codes: 160.3918, 110.2760.

Metamaterials (MTMs) have strong abilities to manipulate electromagnetic (EM) waves on a subwavelength scale, resulting in fascinating effects such as negative refraction [1], superimaging/hyperimaging [2–4], and anomalous reflection/refraction [5]. Inspired by Pendry's super lens [2] that could focus a *point* source to a *point* image, many efforts were devoted to utilizing MTM lenses to focus a *plane* wave (PW) to a *point* image [6–14]. Conventional lenses to achieve this goal typically exhibit certain curved shapes and thus are *bulky* in size and difficult to fabricate [15]. Recently, several MTM-based lenses, working in transmission geometry, were proposed in microwave [6–8], terahertz [9,10], and visible frequency domains [11–14]. The common idea behind these works is to carefully engineer the refraction-index distributions, so that waves transmitted through these MTM lenses at different lateral positions can acquire certain phase accumulations, eventually leading to focusing upon wave reinterferences. While these MTM-based lenses are *flat*, they still suffer certain limitations. First, all these lenses were based on engineering the refraction index only, but the impedance-matching problems were generally overlooked. Therefore, they suffer inevitable reflections at the surfaces. Second, these devices cannot be made very thin, since a thinner lens demands a larger index variation, leading to more serious impedance mismatch problems.

Here we propose an alternative MTM lens, operating in *reflection* geometry, to overcome the above issues suffered by previous lenses. Our lens is ultrathin, flat, and can collect all the incoming energy when focusing. Microwave experiments, in good agreement with finite-difference time-domain (FDTD) simulations on realistic samples, are performed to successfully verify the theoretical concept.

In our previous work [16], we showed that a carefully designed metasurface can efficiently control the reflection direction for an input PW. The idea is that a *nonuniform* surface current (SC) $J \propto e^{-i\xi x}e^{i\omega t}$ is created on the metasurface, which generates the oblique reflection beam [16]. However, the reflected wave in that case is still a PW with wavefront unchanged. To achieve a focused beam with a *spherical* wavefront, the generated SC at a local point of the metasurface should carry a phase to compensate the propagation phase between the source and the focal point so that the radiated waves from the metasurface can *constructively* interfere with each other as reaching the focal point [17]. To validate this idea, we assume that the SC

$$\vec{J} = J_0 e^{ik_0\left(\sqrt{x^2+y^2+f^2}-f\right)} e^{i\omega t}\delta(z)\vec{e}_y \tag{1}$$

is generated on an $L \times L$ metasurface located at $z = 0$ and examine its radiation pattern using a dyadic Green's function method (DGFM) [18]. Here $k_0 = \omega/c$, with ω being the frequency, c the light speed, and f the desired focal length. We found that the **E** field radiated from such an SC does converge to the desired focal point $(0, 0, f)$. As an illustration, we show in Fig. 1(a) the computed **E** field patterns on

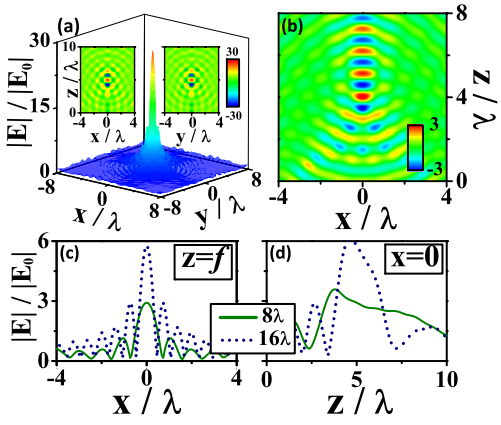

Fig. 1. (Color online) (a) Calculated **E** field pattern on the xy plane with $z = f$ for an SC described by Eq. (1); insets show the $\mathrm{Re}(E_y)$ patterns on two symmetry planes. (b) For an SC described by Eq. (2) with $L = 8\lambda$ and $f = 5\lambda$, calculated $\mathrm{Re}(E_y)$ pattern on the xz plane. For two SCs described by Eq. (2) with $f = 5\lambda$ and different L, calculated **E** distributions on the focal line with $z = f$ (c) and along the center symmetry line (d). All fields are normalized against the field E_0 of a uniform SC, $\vec{J} = J_0 e^{i\omega t}\delta(z)\vec{e}_y$.

the focal plane (with $z = f$) and two symmetry planes (with $x = 0$ and $y = 0$) [19], respectively, for an SC with $L = 16\lambda$ and $f = 5\lambda$ (λ is the wavelength). That the **E** field is significantly enhanced around the point $(0, 0, f)$ verified the focusing effect.

We next consider a simplified case that is easy to realize experimentally. Suppose the SC generated on the metasurface (sized $L \times \infty$) is *uniform* along the y direction and is modulated only along the x direction; then we have

$$\vec{J} = J_0 e^{ik_0\left(\sqrt{x^2+f^2}-f\right)} e^{i\omega t}\delta(z)\vec{e}_y. \tag{2}$$

Applying the DGFM [18] again, we numerically calculated the **E** fields radiated from such a simplified SC (with $L = 8\lambda$ and $f = 5\lambda$). Field distribution on the xz plane [see Fig. 1(b)] shows that EM wave radiated from the SC does converge to a focal line. We depicted in Figs. 1(c) and 1(d) the calculated field distributions along the x axis (with $z = f$) and the center symmetry line (with $x = 0$), respectively. While the peak is reasonably narrow in Fig. 1(c), it is quite broad in Fig. 1(d), and the focal length is more accurately identified as $f' = 3.8\lambda$, shorter than the designed value $f = 5\lambda$. We found such discrepancies are caused by the finite-size effect. We repeated all calculations for a larger lens with $L = 16\lambda$ and depicted the obtained results in Figs. 1(c) and 1(d). Comparison between the two cases (i.e., $L = 8\lambda$, 16λ) shows that the focusing effect is significantly improved and the focal length is approaching more to f as L increases. We note that our focusing is not subwavelength, since here we are in the far field where evanescent fields cannot reach the focal line.

We now design realistic systems that can support the SC as defined in Eq. (2) when illuminated by a normally incident PW. Consider a *homogeneous* metasurface that *perfectly* reflects EM waves but with a reflection phase Φ (i.e., $r = e^{i\Phi}$ is the reflection coefficient of the electric field), then the SC generated on the metasurface (illuminated by a normally incident PW) must take the same phase Φ ($J \propto e^{i\Phi}$) [18]. Extend to the *inhomogeneous* case, we understand that the desired metasurface should exhibit a parabolic reflection-phase profile

$$\Phi(x) = \Phi_0 + k_0\sqrt{x^2+f^2} - k_0 f \tag{3}$$

for an incident EM wave with polarization $\vec{E}\|\hat{y}$ at frequency ω. Equation (3) is the key result of our Letter. Among many possibilities, here we present one design for the metasurfaces based on high impedance surface (HIS) structures [20,21]. The building block consists of a metallic "H" and a continuous metal sheet separated by a 1.6 mm thick dielectric layer with $\varepsilon_r = 4.2$ [see inset to Fig. 2(a)]. A system consisting of an array of *identical* unit elements is the usual HIS, which perfectly reflects EM waves but with Φ sensitively depending on structural parameters. FDTD simulations [22] [solid line in Fig. 2(a)] show that Φ calculated at 10 GHz for such an HIS can be tuned easily from π to $-\pi$ by changing the parameter L_y from 1 to 4 mm. We fabricated seven HIS samples with different L_y and measured their reflection phases.

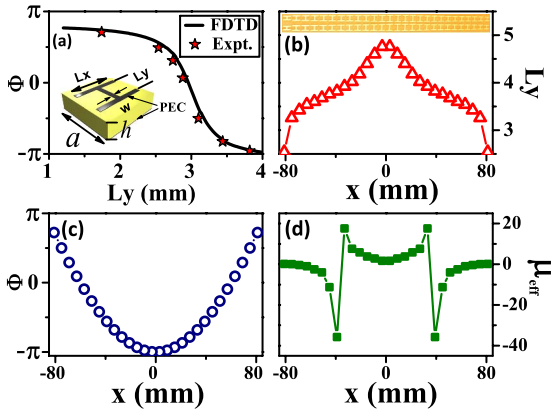

Fig. 2. (Color online) (a) Reflection phase (Φ) versus L_y for HISs with unit cell shown in the inset, obtained by FDTD simulations and experiments. Other parameters are $a = 6$ mm, $h = 1.6$ mm, $w = 0.5$ mm, and $L_x = 5$ mm. (b) L_y versus position x for the designed metasurface; inset shows a picture of real sample. (c) FDTD-calculated $\Phi(x)$ profile. (d) Retrieved $\mu_{\text{eff}}(x)$ profile of the designed metasurface.

Experimental results are in good agreement with FDTD simulations [Fig. 2(a)].

Via carefully selecting the L_y value of each unit, we successfully designed a planar metasurface exhibiting a parabolic $\Phi(x)$ profile [Eq. (3)] with $f = 100$ mm. Figure 2(b) shows how L_y in different "H" varies as a function of position x, and Fig. 2(c) depicts the FDTD-simulated $\Phi(x)$ profile of the designed metasurface. A 162 mm × 12 mm sample was fabricated based on the design, part of which is shown in the inset to Fig. 2(b). Inserting the sample into a parallel-plate waveguide and shining the metasurface with a y-polarized plane microwave (transverse-EM mode of the waveguide) at frequency 10 GHz, we adopted a near-field scanning technique [see Fig. 3(a) for the experimental setup; more details can be found in [23] to map the distribution of electric fields scattered by the metasurface. The spatial

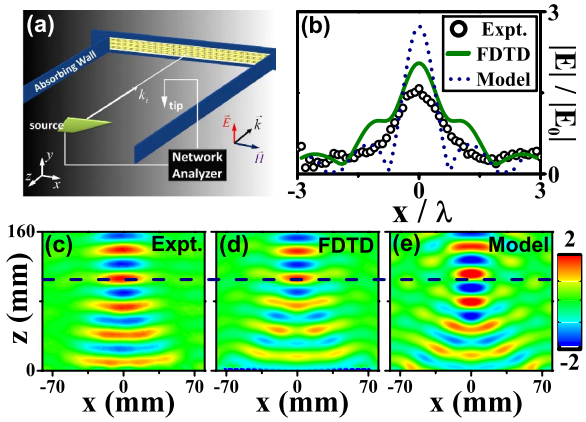

Fig. 3. (Color online) (a) Sketch for the experimental setup. (b) **E** field distributions along the focal line, obtained by experiment and FDTD simulations on realistic samples and on the model system. (c) Re(E_y) on the xz plane, obtained by experiment, FDTD simulations (d) on realistic sample and (e) on the model system. The dashed line denotes the designed focal line ($f = 100$ mm). All fields are normalized against the input field strength, and the metasurface is placed at the $z = 0$ plane.

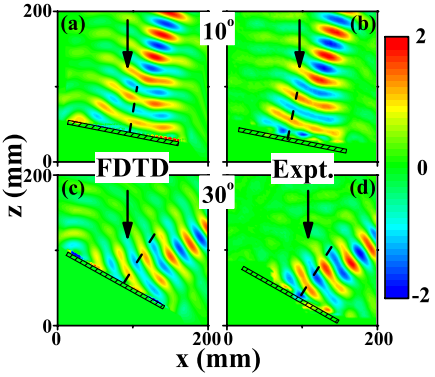

Fig. 4. (Color online) Re(E_y) patterns obtained by FDTD simulations and experiments as the metasurface is illuminated by TE-polarized microwaves at incident angles (a), (b) $\theta_i = 10°$ and (c), (d) $\theta_i = 30°$. All fields are normalized against the input field strength.

resolution of the mapping is 2 mm, and both amplitude and phase of the electric field were recorded by a vector network analyzer (Agilent N5230C). To illustrate the focusing effect more clearly, we purposely deducted the incident field from the total field to obtain the pure information of the scattered field. We also performed FDTD simulations on the realistic structure to compute the scattered-field pattern. Figures 3(c) and 3(d) depict the experimentally measured and FDTD-calculated scattered-field patterns, respectively, both showing that the scattered EM field does converge to a focal line located at $z \approx 80$ mm where the field is maximized. The focal length is shorter than the predesigned value ($f = 100$ mm), which can be explained by the finite-size effect [see Fig. 1(d)]. Along the focal line defined at $z = 80$ mm, we measured and simulated the field distributions and compared the results in Fig. 3(b). The common pronounced peak at the origin in both spectra reinforced the expected focusing effect.

To gain a deeper understanding on the noted effect, we derived an effective medium model for the designed metasurface. According to [21], we found the metasurface can be modeled as a magnetic slab with effective permeability $\mu_{\text{eff}}(x)$ [24] put on a perfect electric conductor. By comparing Φ calculated based on the realistic HIS and the model system, we successfully retrieved the $\mu_{\text{eff}}(x)$ profile of the model system [see Fig. 2(d)]. The scattered-field patterns calculated based on such a model are shown in Figs. 3(b) and 3(e), which are in good agreement with both experiments and full wave simulations.

Our lens also works for oblique-incidence cases. Figure 4 compares the scattered-field patterns obtained by experiments and simulations for two oblique incident angles (10°, 30°). Good agreement between experiments and simulations is noted. The focusing effect becomes worse as θ increases, since the $\Phi(x)$ profile may change slightly for the oblique-incidence case. However, the focusing effect is still observable for $\theta = 30°$ [see Figs. 4(c) and 4(d)] and simulations show that the effect survives up to $\theta = 45°$ (not shown). In addition, we can also realize the defocusing effect upon carefully designing a metasurface with $f < 0$ in which the incoming PW becomes a divergent beam with a virtual focal point behind the lens. Finally, although here we only experimentally verified the focusing effect in a simplified version [based on Eq. (2)], we note that extensions to more complicated cases are straightforward.

In conclusion, we demonstrated that an ultrathin flat metasurface with a parabolic reflection-phase profile can focus an incident PW to a point image with high efficiency.

This work was supported by NSFC (60990321, 11174055, 60990324, and 11204040) and the Program of Shanghai Subject Chief Scientist (12XD1400700).

References and Notes

1. R. A. Shelby, D. R. Smith, and S. Schultz, Science **292**, 77 (2001).
2. J. B. Pendry, Phys. Rev. Lett. **85**, 3966 (2000).
3. N. Fang, H. Lee, C. Sun, and X. Zhang, Science **308**, 534 (2005).
4. Z. Liu, H. Lee, Y. Xiong, C. Sun, and X. Zhang, Science **315**, 1686 (2007).
5. N. Yu, P. Genevet, M. A. Kats, F. Aieta, J. P. Tetienne, F. Capasso, and Z. Gaburro, Science **334**, 333 (2011).
6. Q. Lin, T. J. Cui, J. Y. Chin, X. M. Yang, Q. Cheng, and R. Liu, Appl. Phys. Lett. **92**, 131904 (2008).
7. R. Liu, X. M. Yang, J. G. Gollub, J. J. Mock, T. J. Cui, and D. R. Smith, Appl. Phys. Lett. **94**, 073506 (2009).
8. N. Kundtz and D. R. Smith, Nat. Mater. **9**, 129 (2009).
9. O. Paul, B. Reinhard, B. Krolla, R. Beigang, and M. Rahm, Appl. Phys. Lett. **96**, 241110 (2010).
10. J. Neu, B. Krolla, O. Paul, B. Reinhard, R. Beigang, and M. Rahm, Opt. Express **18**, 27748 (2010).
11. L. Verslegers, P. B. Catrysse, Z. Yu, J. S. White, E. S. Barnard, M. L. Brongersma, and S. Fan, Nano Lett. **9**, 235 (2009).
12. L. Lin, X. M. Goh, L. P. McGuinness, and A. Roberts, Nano Lett. **10**, 1936 (2010).
13. C. Ma and Z. Liu, Appl. Phys. Lett. **96**, 183103 (2010).
14. C. Ma, M. A. Escobar, and Z. Liu, Phys. Rev. B **84**, 195142 (2011).
15. M. Born and E. Wolf, *Principles of Optics* (Cambridge University, 1999).
16. S. Sun, Q. He, S. Xiao, Q. Xu, X. Li, and L. Zhou, Nat. Mater. **11**, 426 (2012).
17. We neglected the amplitude differences of waves radiated from the SC at different local positions. We expect that it may not significantly influence the focusing effect since field radiated from a point (line) source varies slowly versus $r(E(r) \propto r^{-1}, \ln(r))$.
18. L. Zhou, X. Q. Huang, and C. T. Chan, Photonics Nanostruct. Fundam. Appl. **3**, 100 (2005).
19. Some of calculated/measured field patterns are for Re(E_y) (with phase included) so that wave propagations can be easily identified.
20. D. Sievenpiper, L. Zhang, R. Broas, N. G. Alexopolous, and E. Yablonovitch, IEEE Trans. Microw. Theory Technol. **47**, 2059 (1999).
21. J. M. Hao, L. Zhou, and C. T. Chan, Appl. Phys. A **87**, 281 (2007).
22. Simulations were performed using the EastFDTD v2.0 Beta, DONGJUN Science and Technology Co., China.
23. B. J. Justice, J. J. Mock, L. Guo, A. Degiron, D. Schurig, and D. R. Smith, Opt. Express **14**, 8694 (2006).
24. The magnetic slab represents the region occupied by the spacer and the upper metal sheet, with a total thickness of 1.65 mm.